Two-dimensional layered materials of rare-earth Er-doped MoS₂ with NIR-to-NIR down- and up-conversion photoluminescence

Gongxun Bai, Shuoguo Yuan, Yuda Zhao, Zhibin Yang, Sin Yuk Choi, Yang Chai, Siu Fung Yu, Shu Ping Lau, and Jianhua Hao*

G. X. Bai, S. G. Yuan, Y. D. Zhao, Z. B. Yang, S. Y. Choi, Prof. Y. Chai, Prof. S. F. Yu, Prof. S. P. Lau, and Prof. J. H. Hao
Department of Applied Physics, The Hong Kong Polytechnic University, Hong Kong, P. R. China
E-mail: jh.hao@polyu.edu.hk

Keywords: upconversion, 2D materials, substitution doping, rare-earth ions, photoluminescence

Atomically thin layered materials have attracted remarkable scientific and technological interest.[1] The layered structure in bulk consists of the stacking of monolayers by van der Waals-like weak forces. Formation of two-dimensional (2D) forms is promised by the in-plane stability of monolayers supplied by strong covalent bonds. The study of photoluminescence (PL) properties in the single- and few-layer 2D layers has become an important research focus.[2-5] For instance, in 2D transition metal dichalcogenides (TMDs) such as MoS_2, $MoSe_2$, WS_2 and WSe_2, PL measurements have provided experimental evidences to prove the exotic nature of excitons in TMDs.[3,4] Because of the presence of band gap, large exciton binding energies and flexibility, layered TMDs semiconductors are promising for next-generation optoelectronic devices, such as optical sensor, solar cells, displays and light-emitting diodes (LEDs).[6,7] However, the primary emissions of PL or electroluminescence (EL) observed in all 2D TMDs materials and devices are currently limited to the spectral range from visible to the edge of near-infrared (NIR). So far, tuning of luminescence is restricted by the excitons, energy band gap and layer numbers of 2D semiconductors. Apparently, it should be very attractive for the fundamental study and application of 2D materials if the luminescence can be extended to a wide range of NIR

1 spectrum, e g , telecommunication range (1 55 μm) [7] In theory, chemical doping can

2 potentially modify the functionality of TMDs by providing routes to tune their intrinsic

3 properties, e.g., changing semiconductor from n- to p-type, achieving tunable p-n junction,

4 modifying band structure, chemical sensitivity and magnetism, etc. Specifically, Dolui *et al.*

5 proposed possible doping strategies for MoS_2 monolayers through an *ab initio* calculation

6 study.[8] In the past few years, some researchers have conducted experiments to modify the

7 properties of TMDs with the doping strategies.[9-15] The doping of MoS_2 with manganese

8 (Mn) was performed,[9] and the introduction of Mn into MoS_2 lattices may lead to the changes

9 in the band structure and PL emission. An approach to engineer optical band gap was

10 proposed via selenium and other chemical doping in MoS_2,[10,11] while Nb-doped MoS_2 by

11 cation substitution presented p-type transport characteristics used for device construction.[12,13]

12 Additionally, other doping MoS_2 elements have been shown, such as Re,[14] and Au[15].

13 Unfortunately, among the existing doping approaches, the emission peak is only extended

14 from 652 nm of pristine MoS_2 to 681 nm of Mn-doped MoS_2. [9] Hence, it is striking to find a

15 solution to tune the luminescence of 2D semiconductors more effectively.

16   By contrast, it is noticeable that rare-earth (RE) ions commonly doped in traditional

17 insulator or semiconductor hosts have abundant excited energy levels with unique intra 4f

18 electronic transitions that enables them to absorb and emit photons from ultraviolet (UV) to

19 infrared region.[16-20] The luminescence features of RE ions include high quantum yield,

20 narrow bandwidth, long-lived emission, high photostability and large Stokes shifts. Typically,

21 Er-doped fibers and semiconductors are capable of emitting sharp luminescence lines near

22 1500 nm,[21] which is essential for modern optical communication and optoelectronic devices.

23 Interestingly, new developments have been made from RE-doped nanoparticles, leading to

24 promising applications in biological and optoelectronic fields.[22,23] The nanostructural hosts

25 have resulted in the implementation of a new platform for investigating novel PL features of

26 RE dopants, such as upconversion (UC) where many new phenomena associated with energy

2

migration have recently been found and photon management tasks can be addressed.[23-26] Unfortunately, there has been no report on introducing RE ions into the new family of nanoscale structures, *i.e.* 2D TMDs semiconductors. Therefore it is unknown to what effects can bring to 2D materials. Such studies raise intriguing questions whether RE ions are capable of introducing energy levels within the bandgap of 2D semiconductors and hence give out desired emissions, e.g. expanded emission via various energy transfer pathways of RE ions. In this work, we will take advantage of typical Er ions and apply them to the large-scale 2D MoS_2 thin films synthesized by chemical vapor deposition (CVD) technique. Both UC and downconversion (DC) PL emissions located in NIR spectral regime are first observed in 2D layered TMDs simply using a single wavelength NIR pumping source. Consequently, luminescence wavelengths of the RE-doped 2D TMDs have been greatly extended and tuned compared to pristine counterpart.

Figure 1a shows the sulfurization of Er-doped Mo thin film by CVD method. Briefly, followed by the film deposition, the as-grown film samples were placed in the center of a tube quartz furnace. Another ceramic boat holding high purity sulfur powder (>99.99 %) was mounted in the upwind low-temperature zone of the tube. During the synthesis, the temperature in the low-temperature zone was controlled to be slightly above the melting point of sulfur (120 °C). The quartz tube was kept in a flowing protective Ar gas. Figure 1b shows an optical image of the prepared Er-doped MoS_2 on a SiO_2/Si substrate. The as-prepared samples can serve for the subsequent structural characterization and PL measurements as shown in Figure 1c.

We have investigated microstructures, doping profile, layered structures, and cross-sectional interface of the fabricated thin films using high-resolution transmission electron microscopy (HR-TEM) and X-ray photoelectron spectroscopy (XPS). **Figure 2**a shows the HR-TEM image of the MoS_2:Er, indicating that the layered structure is preserved when Er ions are doped in MoS_2. Fast Fourier transform (FFT) pattern in the inset of Fig. 2a confirms

3

1   the crystal structure and crystalline of the sample. To identify the location of Er dopant within

2   MoS_2, the samples were further characterized by high-angle annular darkfield scanning

3   transmission electron microscopy (HAADF-STEM) with the correction of spherical (CS)

4   aberration (Figure 2b, c). Because of the difference in atomic number (Z) in S (Z=14), Mo

5   (Z=42) and Er (Z=68), Er atoms marked by white circles can be imaged in Figure 2b and 2c.

6   Since HAADF intensity is proportional to Z, the Er atoms show stronger intensity in HAADF

7   compared to Mo (Figure 2d). The energy dispersive X-ray spectroscopy (EDS) in Figure 2e

8   implies the existence of Er atom with the Er/Mo ratio of about 3% in the sample on TEM Cu

9   grid. Figure 2f and 2g show the comparisons of XPS results from the CVD grown undoped

10   MoS_2 (in red) and MoS_2:Er (in blue). It is seen that the core-level peaks of Mo and S in the

11   MoS_2:Er sample present a uniform shift towards lower binding energies compared to those of

12   the undoped MoS_2 (Figure 2f), indicating the change in chemical micro-environment. These

13   results reveal that such a binding energy difference is associated with a Fermi level shift,

14   which is a clear evidence for incorporation of Er into the Mo-based lattices. As expected, the

15   distinct binding energy peaks corresponding to Er $4d$ core-levels at 172.6 and 168 eV were

16   detected only in the MoS_2:Er sample (Figure 2g). And it well matches the previously observed

17   XPS features from $NaGdF_4$:Yb,Er nanoparticles (Er $4d$, 172.68 eV)[27] and $ErSi_{1.7}$ thin films

18   (Er $4d$, ~168 eV)[28]. It implies that the incorporation of Er into the MoS_2 lattices essentially

19   preserves the Er^{3+} state. The typical value of binding energy peak $4p3/2$ for Er_2O_3 is 320.1

20   eV[29]. No obvious binding energy peaks of Er_2O_3 can be recognized here. The TEM and XPS

21   results provide clear evidences that Er atoms are incorporated into MoS_2 lattice via

22   substitional cation doping rather than surface adsorption or decoration.

23   Followed by the structural characterization, we have further measured Raman and PL

24   spectra of the prepared MoS_2:Er samples. **Figure 3**a presents Raman spectra of the prepared

25   layered MoS_2 and MoS_2:Er under 488 nm excitation (Horiba Jobin Yvon HR800). The peak

26   spacing between E^1_{2g} and A_{1g} is 22.3 cm^{-1}, further evidencing the bilayer structure mainly

1　existed in our samples illustrated by the above TEM measurement. The Raman peaks in

2　MoS_2:Er shift 2 cm^{-1}, implying the possible effects of the light Er doping and/or the presence

3　of defects on 2D MoS_2 structure.[30] Figure 3b shows PL spectra of the bilayer samples under

4　488 nm (2.58 eV which is larger than the band gap of 2D MoS_2) excitation. The PL signal of

5　MoS_2:Er is located at 667 nm (1.86 eV), similar to the result of pristine MoS_2.

6　Under the excitation at 980 nm with a continuous-wave (CW) diode laser, some interesting

7　PL results were found. As shown in **Figure 4**a, the UC emission at about 800 nm was

8　observed in MoS_2:Er nanosheets pumped by the diode laser with an excitation density of 0.5

9　W/mm^2. Note that other emission peaks at shorter wavelength were not observed. It is

10　deduced that radiative transitions with higher photon energies than MoS_2 bandgap (1.86 eV)

11　are absorbed by the host. The inset is the pump power (P) dependence at 980 nm of the PL

12　intensity (I) at 800 nm. The slope (n) of $I \propto P^n$ is fitted to be around 1.57, indicating the UC

13　emission is a two-photon process. To date, UC nanoparticles have been extensively reported

14　for promising applications in biomedicine.[17-19,22] In particular, some NIR-to-NIR

15　luminescence within the so-called biological optical window is of great interest for

16　bioimaging and biodetection due to the low absorption and scattering from tissues. Very

17　recently, 2D layered materials (e.g., MoS_2, WS_2) have also been considered for the potential

18　applications in biomedicine.[31] The results as shown in Figure 4a suggest that MoS_2:Er with

19　NIR-to-NIR UC emission has unprecedented advantages in these potential 2D applications.

20　The mapping image of UC PL spectra in terms of both position and intensity from MoS_2:Er

21　sample is shown in Figure 4b**.** The result suggests an uniform coverage and luminescence

22　profile of MoS_2:Er atomic layers on the SiO_2/Si substrate in terms of spatial distribution. In

23　addition to the finding of UC PL, the DC emission was simultaneously observed at ~1550 nm

24　in the MoS_2:Er pumped at 980 nm with an excitation density of 0.5 W/mm^2 (Figure 4c). The

25　emission processes of Er^{3+} ions result in both UC and DC transitions due to the energy

26　transitions ascribed to Er^{3+} ions. As shown in Figure 4d, the slope (n) of pump power (P) at

5

1 980 nm and PL intensity (*I*) at 1550 nm is 1.23, indicating that the population for $^4I_{13/2}$ mainly

2 comes from a one-photon process. It is well known that 1550 nm low loss window is most

3 widely used in optical communication and photonic technologies. In fact, the ultimate goal of

4 making atomically thin electronic and optoelectronic devices triggers the current intensive

5 research on 2D nanosheets. Therefore, the results as shown in Figure 4c indicate that Er-

6 doped MoS_2 not only yields significantly expanded luminescence of 2D TMDs to NIR range

7 beneficial to fundamental research, but also brings a new opportunity to the development of

8 atomically thin NIR devices pumped by a commercial diode laser. It should be emphasized

9 that no such NIR-to-NIR UC and DC emissions were observed in pristine MoS_2 samples

10 under identical test condition as indicated in Figure 4a and 4c.

11 To provide an in-depth understanding of the measured results on the novel NIR-to-NIR

12 down- and up-conversion PL, density functional theory (DFT) calculations were performed

13 on the 2D bilayered MoS_2:Er (**Figure 5**a and 5b). DFT calculations were implemented in

14 Quantum ESPRESSO.[32] The exchange correlation energy is described by the generalized

15 gradient approximation. The 4×4 conventional unit cell is used for the pristine MoS_2 and Er-

16 doped MoS_2 bilayer. The detailed calculation method is presented in the experimental part.

17 The stability of Er doping MoS_2 is described by the binding energy between Er and MoS_2

18 ($E_{binding}$). $E_{binding}$ is defined as

19

$$E_{binding} = E_{Er\text{-}MoS2} - E_{Mo\text{-}defect} - E_{Er} \qquad (1)$$

21

22 where $E_{Er\text{-}MoS_2}$ is the energy of Er doped MoS_2 system, $E_{Mo\text{-}defect}$ is the energy of MoS_2 system

23 and E_{Er} is the energy of individual Er atom.

24 The calculated result is shown in Figure 5c. When Er atom passivates the Mo vacancy, the

25 system will be more stable and release 1.78 eV energy. It implies that the system remains

26 stable in terms of the density of states when Er is doped into MoS_2 lattice by cation

6

substitution. Importantly, the Er substitution can introduce the density of states within the bandgap of MoS_2, which offers the possibility of inducing additional energy transition leading to NIR luminescence. Considering the energy levels of Er^{3+},[23] the energy band diagram of our synthesized MoS_2:Er system is illustrated as shown in Figure 5d. Er^{3+} features a ladder of nearly equally spaced energy levels, which is an ideal candidate as optical activator widely used for producing NIR up- and down-conversion emissions. According to UC mechanism, the NIR photons at about 800 nm ascribed to the energy transition of $^4I_{9/2}$ ---$^4I_{15/2}$ are capable of emit and transmit within the bandgap of MoS_2 when the photons at 980 nm are absorbed sequentially. Meanwhile, the most investigated 1550 nm emission ascribed to the energy transition of $^4I_{13/2}$ ---$^4I_{15/2}$ can be observed based on DC process. Indeed, our PL measurements as shown in Figure 4a and 4c match the proposed energy band diagram of MoS_2: Er well.

In summary, we have designed and synthesized novel 2D system of Er-doped MoS_2 layered nanosheets. Structural studies indicate that the Er atoms can be substitutionally introduced into MoS_2 by replacing the Mo cations in 2D host lattice to form stable doping. DFT calculation implies that the Er substitution can introduce the density of states within the bandgap of MoS_2. Both NIR-to-NIR UC and DC light-emissions are first observed in 2D TMDs, ascribed to the energy transition from Er^{3+} dopants. Importantly, the luminescence of 2D materials simply pumped by a single CW laser diode at 980 nm can be extended to a wide range of NIR spectrum, including telecommunication range at 1 55 μm By considering the abundant energy levels arisen from RE ions, our works open a door to greatly extend and modulate the luminescence wavelengths of 2D semiconductors, which will benefit for not only investigating many appealing fundamental issues, but also developing novel devices.

Experimental Section

First, Er-doped Mo thin films were deposited on SiO_2/Si substrates by sputtering high purity (>99.99%) Er and Mo targets with different power (*e.g.*, Er 5 W, Mo 100 W) to achieve Er

doping into the films. And then Er-doped MoS_2 layered nanosheets were synthesized by CVD method. HAADF-STEM was performed in a JEOL ARM200F with STEM aberration (Cs) corrector operated at 80 kV. At 80 kV the e-beam irradiation effect of sulfur atoms in MoS_2 can be significantly reduced. EDS were collected by Oxford Instruments XMaxN 100TLE 100 mm^2 detector. XPS was carried out using a Physical Electronics 5600 multi-technique system with a monochromated Al Ka source (hv=1486.7 eV). Raman spectra were collected in a Horiba Jobin Yvon HR800 Raman microscopic system with a 488 nm laser. The UC and DC emission spectra and mapping were recorded using an Edinburgh FLSP920 spectrophotometer equipped with a commercial CW 980 nm laser diodes and Nikon microscope Eclipse Ti.

Density Function Theory Calculations: The self-consistent field calculation was conducted with Quantum ESPRESSO.[32] The threshold for the convergence on total energy is 10^{-6} and the one on forces was 10^{-3} (both in a.u.). The kinetic energy cutoff for wavefunctions was 50 Ry, and the kinetic energy cutoff for charge density and potential was 200 Ry. The local density approximation (LDA) was adopted in the exchange-correlation energy functional proposed by Perdew-Zunger. The 4×4 conventional unit cell was used for the pristine bilayer MoS_2 and MoS_2:Er, in order to be consist with the doping concentration in the experiment. The vacuum region between adjacent unit cells was set as ~20 Å in the z direction. And a 4×4×1 k-point sampling was used for mesh setting.

Received: ((will be filled in by the editorial staff))
Revised: ((will be filled in by the editorial staff))
Published online: ((will be filled in by the editorial staff))

8

1

[1] R. F. Service, *Science* **2015**, *348*, 490-492.

[2] Z. Yin, X. Zhang, Y. Cai, J. Chen, J. I. Wong, Y.-Y. Tay, J. Chai, J. Wu, Z. Zeng, B. Zheng, H. Y. Yang, H. Zhang, *Angew. Chem. Int. Edit.* **2014**, *53*, 12560-12565.

[3] A. Splendiani, L. Sun, Y. B. Zhang, T. S. Li, J. Kim, C. Y. Chim, G. Galli, F. Wang, *Nano Lett.* **2010**, *10*, 1271-1275.

[4] G. Eda, H. Yamaguchi, D. Voiry, T. Fujita, M. W. Chen, M. Chhowalla, *Nano Lett.* **2011**, 11, 5111-5116.

[5] W. Jie, X. Chen, D. Li, L. Xie, Y. Y. Hui, S. P. Lau, X. Cui, J. Hao, *Angew. Chem.* **2015**, *127*, 1201-1205.

[6] D. Jariwala, V. K. Sangwan, L. J. Lauhon, T. J. Marks, M. C. Hersam, *ACS nano* **2014**, *8*, 1102-1120.

[7] F. Xia, H. Wang, D. Xiao, M. Dubey, A. Ramasubramaniam, *Nat. Photon.* **2014**, *8*, 899-907.

[8] K. Dolui, I. Rungger, C. Das Pemmaraju, S. Sanvito, *Phys. Rev. B* **2013**, *88*.

[9] K. Zhang, S. Feng, J. Wang, A. Azcatl, N. Lu, R. Addou, N. Wang, C. Zhou, J. Lerach, V. Bojan, M. J. Kim, L. Q. Chen, R. M. Wallace, M. Terrones, J. Zhu, J. A. Robinson, *Nano Lett.* **2015**, *15*, 6586-6591.

[10] Y. Gong, Z. Liu, A. R. Lupini, G. Shi, J. Lin, S. Najmaei, Z. Lin, A. L. Elías, A. Berkdemir, G. You, *Nano Lett.* **2013**, *14*, 442-449.

[11] S. Mouri, Y. Miyauchi, K. Matsuda, *Nano Letters* **2013**, *13*, 5944-5948.

[12] J. Suh, T.-E. Park, D.-Y. Lin, D. Fu, J. Park, H. J. Jung, Y. Chen, C. Ko, C. Jang, Y. Sun, R. Sinclair, J. Chang, S. Tongay, J. Wu, *Nano Lett.* **2014**, *14*, 6976-6982.

[13] S. Das, M. Demarteau, A. Roelofs, *Appl. Phys. Lett.* **2015**, *106*.

[14] Q.-C. Sun, L. Yadgarov, R. Rosentsveig, G. Seifert, R. Tenne, J. L. Musfeldt, *ACS Nano* **2013**, *7*, 3506-3511.

1   [15] Y. C. Lin, D. O. Dumcenco, H. P. Komsa, Y. Niimi, A. V. Krasheninnikov, Y. S.

2   Huang, K. Suenaga, *Adv. Mater.* **2014**, *26*, 2857-2861.

3   [16] P. Huang, W. Zheng, S. Zhou, D. Tu, Z. Chen, H. Zhu, R. Li, E. Ma, M. Huang, X.

4   Chen, *Angew. Chem. Int. Edit.* **2014**, *53*, 1252-1257.

5   [17] S. Gai, C. Li, P. Yang, J. Lin, *Chem. Rev.* **2013**, *114*, 2343-2389.

6   [18] K. Binnemans, *Chem. Rev.* **2009**, *109*, 4283-4374.

7   [19] J. Wang, F. Wang, C. Wang, Z. Liu, X. G. Liu, *Angew. Chem. Int. Edit.* **2011**, *50*,

8   10369-10372.

9   [20] V. Mahalingam, F. Vetrone, R. Naccache, A. Speghini, J. A. Capobianco, *Adv. Mater.*

10   **2009**, *21*, 4025-4028.

11   [21] S. Komuro, T. Katsumata, T. Morikawa, X. Zhao, H. Isshiki, Y. Aoyagi, *Appl. Phys.*

12   *Lett.* **2000**, *76*, 3935-3937.

13   [22] M.-K. Tsang, G. Bai, J. Hao, *Chem. Soc. Rev.* **2015**, *44*, 1585-1607.

14   [23] H. Dong, L. D. Sun, C. H. Yan, *Chem. Soc. Rev.* **2015**, *44*, 1608-1634.

15   [24] R. Deng, F. Qin, R. Chen, W. Huang, M. Hong, X. Liu, *Nat. Nano.* **2015**, *10*, 237-242.

16   [25] L. Tu, X. Liu, F. Wu, H. Zhang, *Chem. Soc. Rev.* **2015**, *44*, 1331-1345.

17   [26] D. Q. Chen, Y. S. Wang, M. C. Hong, *Nano Energy* **2012**, *1*, 73-90.

18   [27] P. Ramasamy, P. Chandra, S. W. Rhee, J. Kim, *Nanoscale* **2013**, *5*, 8711-8717.

19   [28] N. Guerfi, T. A. Nguyen Tan, J. Y. Veuillen, D. B. Lollman, Appl. Surf. Sci. **1992**, *56*,

20   501-506.

21   [29] B. D. Paladia, W. C. Lang, P. R. Norris, L. M. Watson, P. J. Fabian, Proc. Roy. Soc. Ser.

22   A **1977**, 354, 269.

23   [30] J. Zheng, H. Zhang, S. Dong, Y. Liu, C. T. Nai, H. S. Shin, H. Y. Jeong, B. Liu, K. P.

24   Loh, *Nat. Commun.* **2014**, *5*, 2995.

25   [31] Y. Chen, C. Tan, H. Zhang, L. Wang, *Chem. Soc. Rev.* **2015**, *44*, 2681-2701.

[32] P. Giannozzi, S. Baroni, N. Bonini, M. Calandra, R. Car, C. Cavazzoni, D. Ceresoli, G. L. Chiarotti, M. Cococcioni, I. Dabo, A. Dal Corso, S. de Gironcoli, S. Fabris, G. Fratesi, R. Gebauer, U. Gerstmann, C. Gougoussis, A. Kokalj, M. Lazzeri, L. Martin-Samos, N. Marzari, F. Mauri, R. Mazzarello, S. Paolini, A. Pasquarello, L. Paulatto, C. Sbraccia, S. Scandolo, G. Sclauzero, A. P. Seitsonen, A. Smogunov, P. Umari, R. M. Wentzcovitch, *J. Phys. Condens. Matter.* **2009**, *21*, 395502.
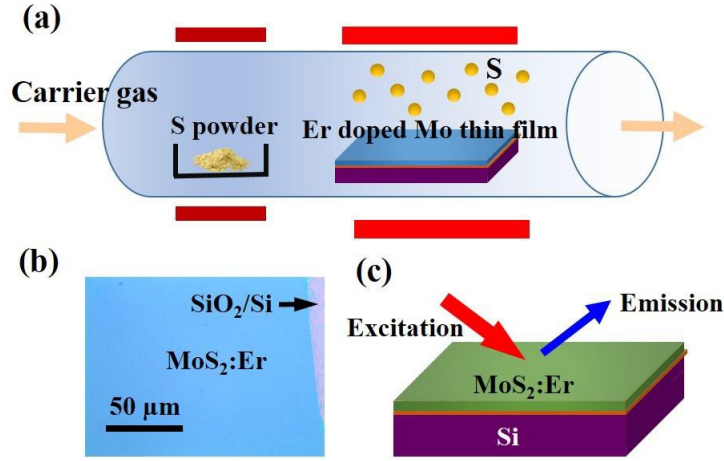
Figure 1. Schematic diagram of synthesis process for the MoS$_2$:Er. (a) Sulfurization of Er-doped Mo thin film pre-deposited by sputtering. (b) The optical image of as-prepared MoS$_2$:Er on Si/SiO$_2$ substrate. (c) PL measurements of MoS$_2$:Er layered nanosheet.
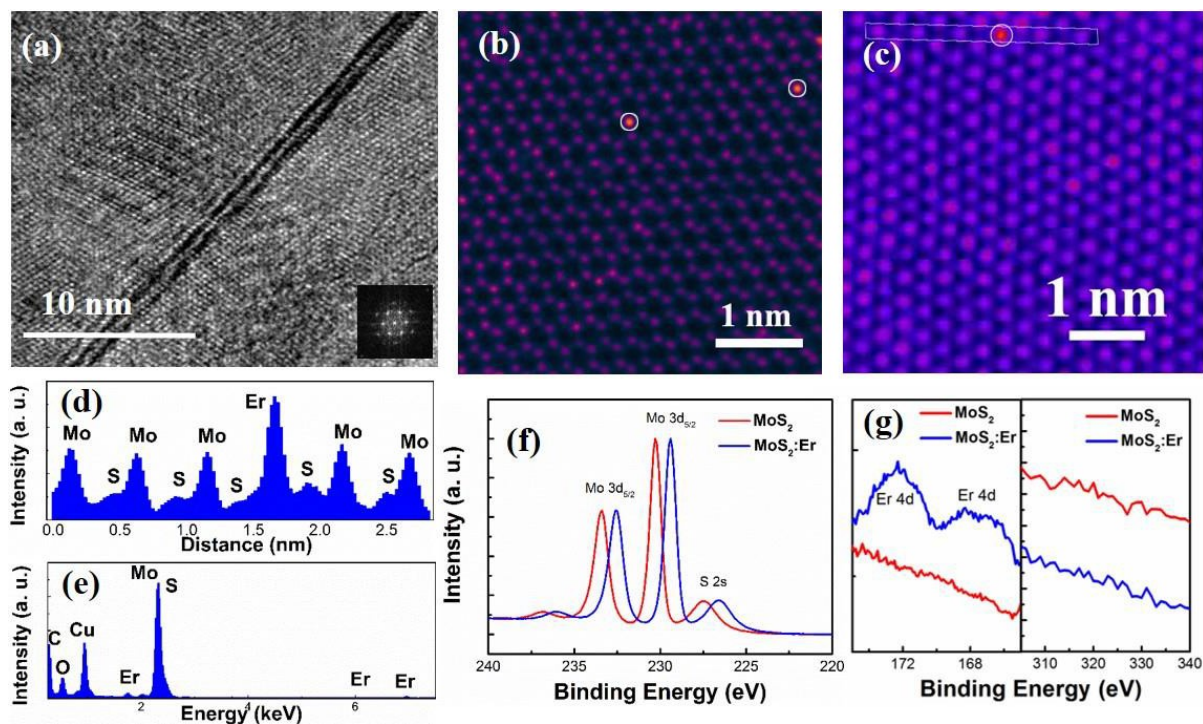
Figure 2. (a) HR-TEM image of MoS_2:Er with bilayer edges. (b) (c) CS-STEM images of the prepared MoS_2:Er sample. The Er atom can be identified from (d) intensity spectra of the selected area where Er atoms show stronger intensity in HAADF compared to Mo. (e) EDS displays a weak Er signal due to the detection limit of EDS. Existence of C, O, and Cu comes from TEM grid. XPS scans of (f) Mo 3d, S 2s, and (g) Er $4d$ core-levels measured from 2D undoped MoS_2 and MoS_2:Er.
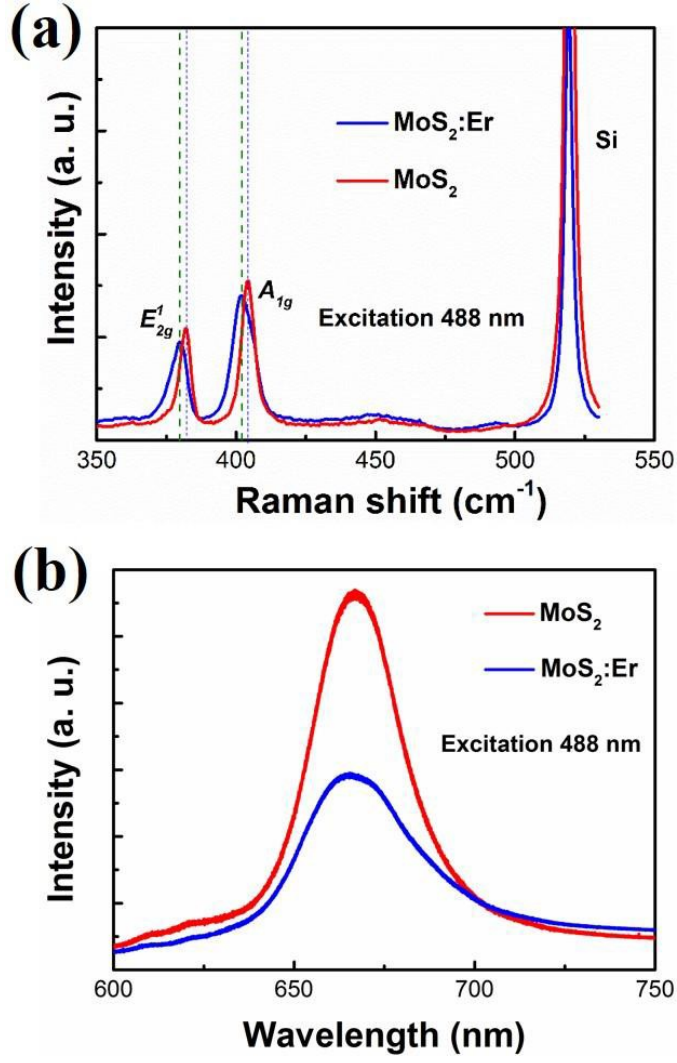
Figure 3. Raman and PL spectra of the prepared MoS$_2$:Er samples. (a) Raman and (b) photoluminescence spectra of bilayer 2D nanosheets on SiO$_2$/Si under 488 nm excitation.
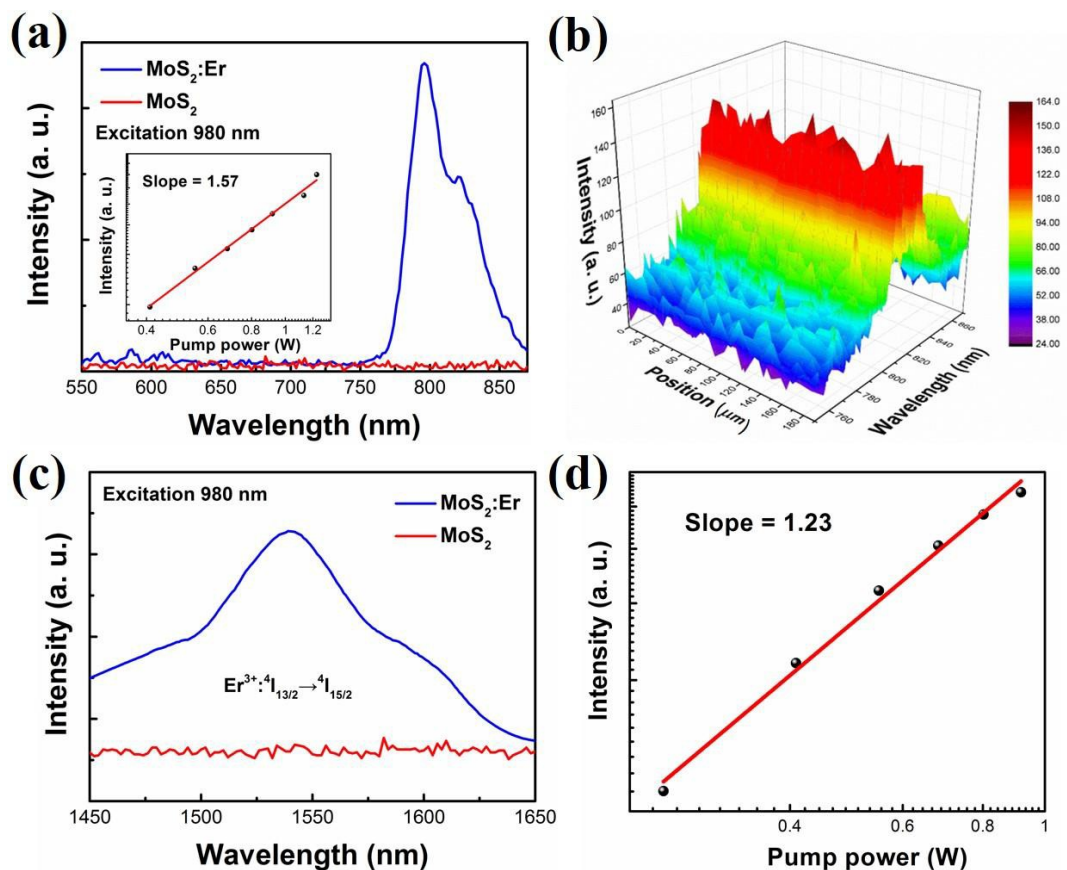
14

Figure 4. (a) NIR UC luminescence with the band peaked at 800 nm of MoS$_2$:Er sample when pumped at 980 nm. The inset is the pump power dependence of PL intensity at 800 nm. (b) The PL spectra mapping image of UC peaks around 800 nm over an area of 200 μm×100 μm. (c) DC PL emitted at around 1550 nm of MoS$_2$:Er thin film when pumped at 980 nm. In (a) and (c) PL spectra of undoped MoS$_2$ thin film are also shown as reference for comparison. (d) The pump power dependence of NIR PL intensity at 1550 nm.
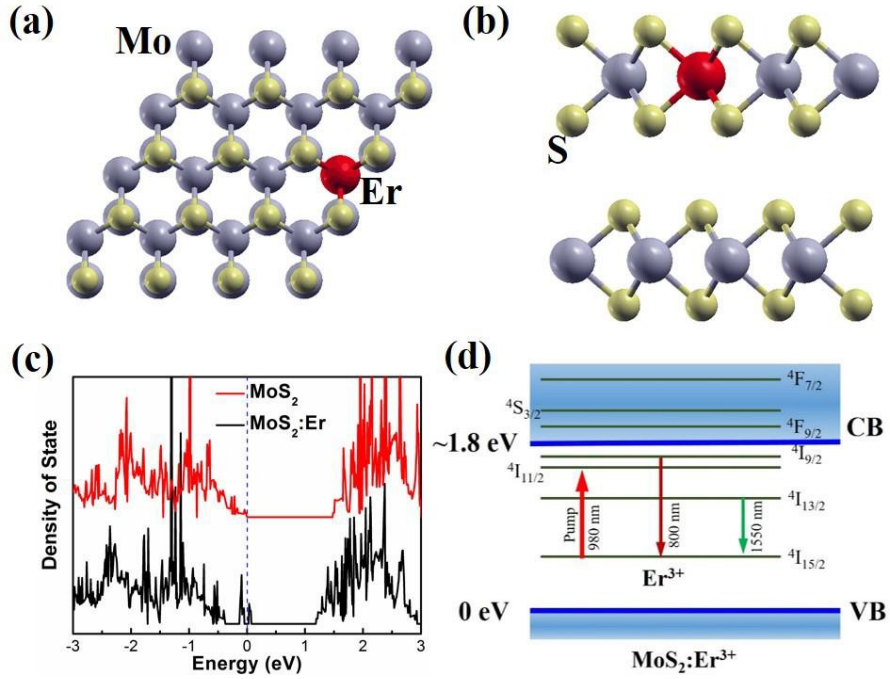
Figure 5. (a) Top view and (b) side view of Er-doped bilayered MoS_2. (c) Density of states (DOS) of the undoped MoS_2 and MoS_2:Er from DFT calculations. (d) Schematic energy level diagram of MoS_2:Er showing sub-bandgap energy transitions ascribed to Er^{3+} dopant, leading to NIR emissions.

A 2D system of Er-doped MoS$_2$ layered nanosheet has been developed. Structural studies indicate that the Er atoms can be substitutionally introduced into MoS$_2$ to form stable doping. DFT calculation implies the system remains stable. Both NIR-to-NIR upconversion and down-conversion light-emissions are observed in 2D TMDs, ascribed to the energy transition from Er^{3+} dopants.

G. X. Bai, S. G. Yuan, Y. D. Zhao, Z. B. Yang, S. Y. Choi, Prof. Y. Chai, Prof. S. F. Yu, Prof. S. P. Lau, and Prof. J. H. Hao*

Two-dimensional layered materials of rare-earth Er-doped MoS$_2$ with NIR-to-NIR down- and up-conversion photoluminescence